ORIGINAL ARTICLE

A Novel IHCP Calculation Scheme to Estimate Surface Heat Flux during Impinging Cooling

Yu-Wei Liu[1] and Chen-Kang Huang[1,*]

[1] *Department of Bio-Industrial Mechatronics Engineering, National Taiwan University, Taiwan*

(**Received** 28 October 2015; **Accepted** 8 December 2015; **Published on line** 1 June 2016)

*Corresponding author: ckhuang94530@ntu.edu.tw

DOI: *10.5875/ausmt.v6i2.1049*

Abstract: This study introduces a novel inverse heat conduction problem (IHCP) calculation scheme to solve the surface heat flux of a subject with impinging cooling. From measured temperature records, the unknown boundary condition can be derived with one of three proposed algorithms. The scheme can then be performed without multiple iterations, and is much faster than traditional methods for IHCP. An impinging cooling apparatus is established to demonstrate the proposed scheme. The apparatus is to experimentally explore three impinging patterns, three impinging positions, and three unknown boundary condition derivation algorithms. The experimental results show that the proposed calculation scheme actually saves calculation time, and provides more accurate results. The most suitable unknown boundary condition derivation algorithm is suggested for each combination of operating parameters.

Keywords: inverse heat conduction problem, IHCP, finite difference, impinging cooling

Introduction

In many industrial applications where the estimation of surface heat flux is important, such as the rocket nozzles [1], engine combustion chambers [2], and furnace casting and hot rolling [3], several concepts for inverse heat conduction problems (IHCP) have been explored to accurately calculate the surface heat flux by modeling the internal heat propagation process.

Surface heat flux is seen as a crucial factor in heat treatment [4]. For example, to enhance both of the efficiency and the performance in the quenching process, an important technique in iron and steel work, the speed and temperature of the quenching process must both be controlled to produce an homogeneous internal temperature profile in a certain period of time. Once the amount of heat flux to be moved for cooling to a certain temperature is known, it is easy to select the most appropriate cooling method. However, heat flux is usually more difficult to measure than temperature. Processing experimental heat flux data requires converting internal temperature profiles to the surface heat flux. This entails an inverse heat conduction problem, since one expects to derive one of the boundary conditions from the solution of the partial differential equation (PDE). In other words, we use a measured temperature matrix to derive the surface heat flux of interest.

The finite element method and finite difference method have been widely applied to boundary value problems [5-7]. The continuous problem domain was discretized, divided into a uniform grid, and then deviated at each point of the problem domain. The Taylor series is widely used to convert the differentiation to simple mathematical form. Numerical methods can then be used to solve the unknown matrix, which stores the distribution to be determined in the domain.

The concept for IHCP was initially introduced to solve heat transfer problems in rocket nozzles [8]. When an IHCP is ill-posed and unstable, any error resulting from this instability will lead to great divergence of the solution. Many studies have provided different solutions for IHCP instability. In 1968, researchers solved one-dimension linear IHCP using a function specification method, and also posed a novel concept of future temperature, combining the least-squares method to stabilize the solution [9]. They then found that the interior temperature reaction would be delayed and damped due

to the change of surface condition [10], leading to the development of the concept of future temperature to estimate surface heat flux and surface temperature. Regarding the determination of unknown surface heat flux, a number of numerical analysis such as graphical and polynomial methods are used to provide continuous and differentiable internal temperature profiles. Based on known data points, various kinds of polynomials combined with interpolation techniques can be used to construct new data points within the range of analysis domain, and to acquire profiles close to the discrete set of known data points.

This paper introduces an improved calculation scheme for IHCP. Three algorithms are used to derive the unknown surface temperature profile according to the thermocouple measurements closest to the impinging surface. The calculated interior temperature profile are then compared with the experimental measurements to verify and validate the effectiveness of the proposed scheme. Also, the performance of the proposed scheme will be compared to that of traditional IHCP methods.

Research method

An experimental apparatus was devised to demonstrate the use of the proposed IHCP calculation scheme. The measured data obtained from the experimental apparatus would provide inputs to the proposed calculation scheme to estimate the calculation error. A cube (60 mm of each side) made of aluminum alloy 6061 was constructed as the test section. One of the six faces of the test section was impinged by pure water, and the other faces were thermally insulated. For simplicity and prompt calculation, calculations were only performed on the central plane vertical to the impinging face. Figure 1 shows the schematic of the experimental apparatus. The vertical plane is the 2D model to be calculated.

For the experimental system described above, the proposed calculation scheme was performed as follows. Figure 2 shows that the rectangular area is divided into m-by-n cells, and superscript p denotes the time step. Circles numbered 1 to 8 denote the thermocouple locations. 3 Arrows denote the 3 impinging positions, one of which is used during each of the test series. Figure 2 shows the model of the nodal network for finite difference formulation of the two-dimensional IHCP calculation. The position indices along the x- and y-axis are respectively expressed as m and n. The first three boundary conditions (top, left and bottom) are assumed to be adiabatic. At each time step, temperatures of the three nodal points, which lie about 3 mm beneath the impinged surface, are used to derive the fourth boundary condition. Consequently, the model runs based on three adiabatic (Neumann) and one temperature-specified (Dirichlet) boundary conditions, as well as initial conditions from previous time steps. The calculated temperature profile for the present time step will be used as the initial condition for the next time step.

Yu-Wei Liu is a Ph.D. candidate in the department of Bio-industrial Mechatronics Engineering, National Taiwan University. His dissertation focuses on energy conservation and environmental controls in plant factory.

Chen-Kang Huang is an associate professor in the department of Bio-industrial Mechatronics Engineering, National Taiwan University. His research interests include heat transfer with phase change, energy engineering, HVAC&R, and plant factory.

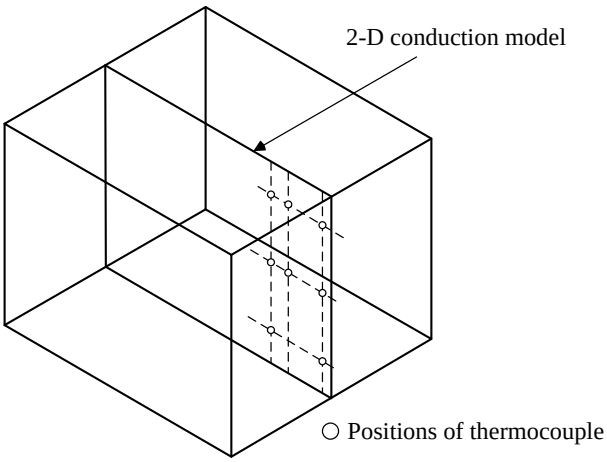

Figure 1. Cross-sectional view of the cube for impinging cooling, where "◯" denotes thermocouple locations. The central vertical plane is the area where 2D conduction calculation is performed.

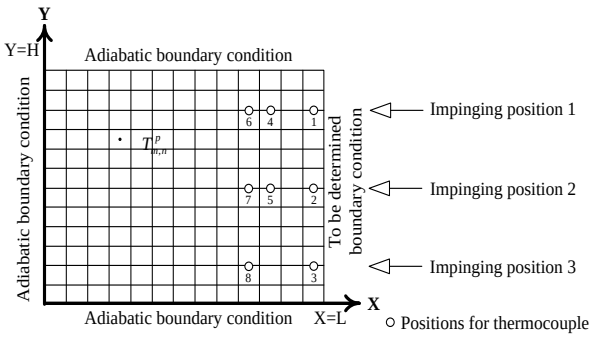

Figure 2. Schematic diagram of the 2D conduction model.

The temperatures of each node can be driven from the general heat conduction equation without internal heat generation as

$$\left(\frac{\partial^2 T}{\partial x^2}+\frac{\partial^2 T}{\partial y^2}\right)=\frac{\partial T}{\alpha\cdot\partial t} \quad (1)$$

where α is thermal diffusivity of the material, and $\alpha=\frac{k}{\rho c}$. Equation (1) can be transformed into a finite difference formulation as Eq. (2)

$$T_{m,n}^{p+1} = \alpha\Delta t\left(\frac{T_{m+1,n}^{p}+T_{m-1,n}^{p}-2T_{m,n}^{p}}{(\Delta x)^2}+\frac{T_{m,n+1}^{p}+T_{m,n-1}^{p}-2T_{m,n}^{p}}{(\Delta y)^2}\right)+T_{m,n}^{p} \quad (2)$$

The three boundary conditions for the left, top and bottom boundary are as follows.

$$\frac{\partial T}{\partial x}=0@x=0 \quad \text{Left side} \quad (3)$$

$$\frac{\partial T}{\partial y}=0@y=0\,\&\,y=H \quad \text{Top and bottom} \quad (4)$$

Three types of impinging patterns—inline jet (flat spray), jet (solid-stream jet), and spray (full-cone spray)—combined with three different impinging positions were applied to perform the calculation scheme, and to evaluate its practical applications. Figure 3 shows photos of the three impinging patterns.

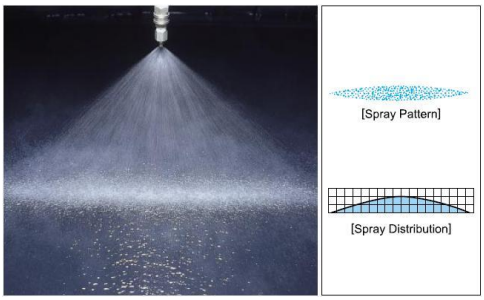

(a) Inline jet (Flat-Spray)

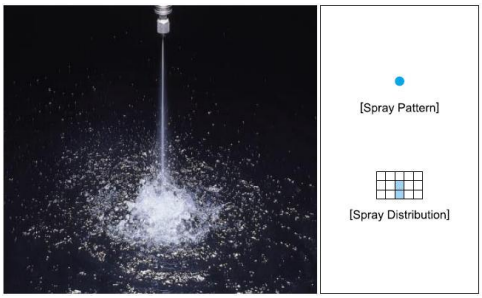

(b) Jet (Solid-Stream Jet)

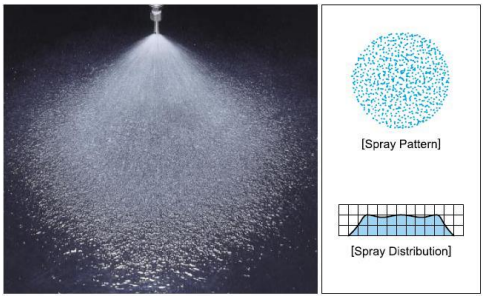

(c) Spray (Full-Cone Spray)

Figure 3. Schematic impinging pattern and flow distribution of (a) inline jet (flat spray), (b) jet (solid-stream jet), and (c) spray (full-cone spray) excerpted from "Catalog on Hydraulic Spray Nozzles" of H. IKEUCHI & Co., LTD.

The heat flux of the impinging surface is to be determined. Traditional IHCP methods take an initial guess for the unknown boundary condition. Many iterations are possibly needed to solve inversed problems. If the fourth boundary condition can somehow be estimated, the problem is no longer inversed and can be solved much faster. This study proposes three similar algorithms to estimate the unknown boundary condition. The three algorithms adapt the measured data located just beneath the impinging surface to correlate the unknown boundary condition.

Algorithm 1 fitted three measured temperatures into a parabolic distribution. The quadratic equation (Eq. 5) can be written as

$$T(Y)=aY^2+bY+c \quad (5)$$

where *Y* is the distance calculated from the bottom. In Algorithm 2, three temperatures were extrapolated and interpolated to derive temperatures of the column just beneath surface. For nodes higher than the thermocouple 1, their temperatures are the same as thermocouple 1. For nodes between thermocouple 1 and 3, their temperatures are linearly interpolated from readings from thermocouple 1 to 3. For nodes lower than thermocouple 3, their temperatures are the same as the thermocouple 3. The algorithm is shown schematically in Figure 4. Algorithm 3 applies the piecewise cubic Hermite interpolation to derive the surface temperature profile. Hermite curves are used to smoothly interpolate between key-points. The basic curve is shown in Fig. 5. The Hermite curves between two points are plotted according to the vector of each point. P1 and P2 are the starting and end points of the Hermite curve. T1 and T2 are the tangent vectors used to determine how the curve leaves the start point and arrives at the end point.

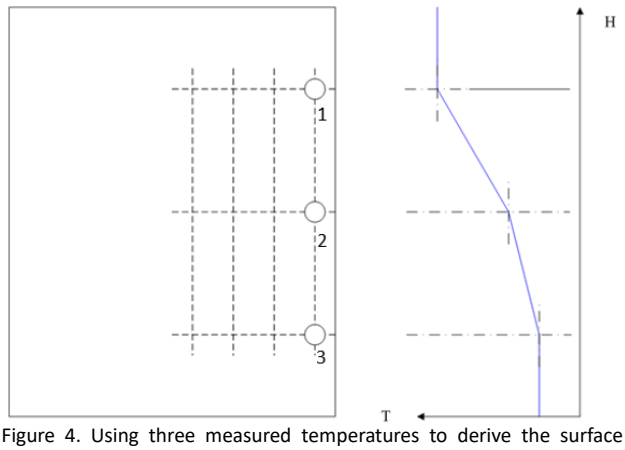

Figure 4. Using three measured temperatures to derive the surface temperature profile (Algorithm 2).

Using one of the three algorithms described above to derive the fourth boundary condition, the nodal

temperatures of every time step can be calculated. The calculation is no longer inversed, and the solution can be found given sufficient boundary conditions. The heat flux of the surface can also be calculated from the energy conservation as Eq. 6.

$$\begin{aligned} &\dot{Q}_{surface} + \frac{k\Delta y}{2}\frac{T^{p}_{m+1,n} - T^{p}_{m,n}}{\Delta x} \\ &+ \frac{k\Delta y}{2}\frac{T^{p}_{m-1,n} - T^{p}_{m,n}}{\Delta x} + \frac{k\Delta x}{2}\frac{T^{p}_{m,n+1} - T^{p}_{m,n}}{\Delta y} \\ &= \rho\frac{\Delta x\Delta y}{2} C\frac{T^{p+1}_{m,n} - T^{p}_{m,n}}{\Delta t} \end{aligned} \quad (6)$$

where $\dot{Q}_{surface}$ (W/m) is the surface heat transfer rate per unit depth normal to the 2D model plane, and p is the time step. The schematic of the derivation of surface heat flux is shown in Fig. 6.

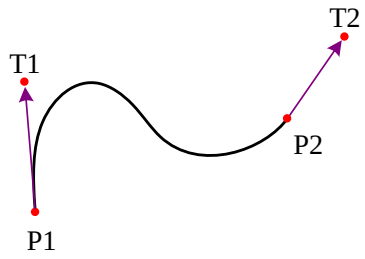

Figure 5. Schematic of the Hermite curve. P1 is the starting point and P2 is the end point. T1 and T2 are vectors for determining curve tangent victors at P1 and P2.

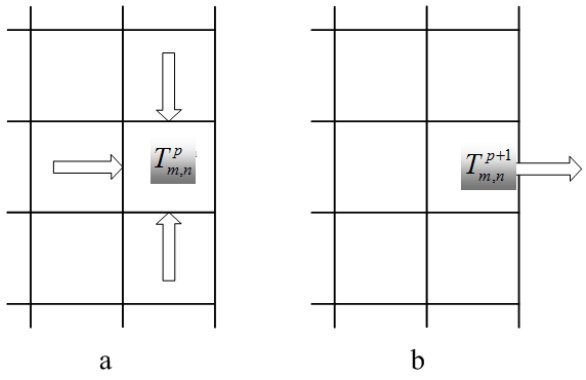

Figure 6. Energy conservation to derive the surface heat flux. (a) Energy entering the element from surrounding elements when t=n and (b) Energy leaving concerned element when next time step t= n+1. [12]

In this study, three impinging positions were explored, labeled as positions 1 to 3 as shown in Fig. 2. Position 1 was the highest (10 mm from the top edge), and position 3 is the lowest (50 mm from the top edge), where position 2 is aligned with the center of the impinging face. The measured data located at the first column were used to perform the unknown boundary condition derivation algorithm. The other data read from thermocouples 4 to 8 are used to compare against the calculated results. The comparison is expressed as the Root Mean Square Error (RMSE) to examine the accuracy of the proposed calculation scheme. RMSE is calculated as follows

$$RMSE = \sqrt{\frac{\sum_{i=1}^{N}(T^{i}_{cal} - T^{i}_{measured})^{2}}{N}} \quad (7)$$

where *N* is the number of total thermocouple readings (N=8 in this study).

Results and discussion

Comparison with traditional solutions for IHCP

Traditional IHCP solutions require initial guesses and many iterations. Therefore, initial guesses for the unknown boundary would be required to solve the present problem using traditional methods. The calculated temperature profile can then be compared to the temperature readings. By iteratively adjusting the fourth boundary condition, the difference between measured temperatures and numerical results can be reduced. The algorithm is iterated to derive the heat flux history over the whole test, second by second. The disadvantage is that these multiple iterations can result in processing time for each one-hundred-second test lasting on the order of ten hours. Also, the minimization scheme could get trapped at a local minimum, instead of a global minimum. If a local minimum is achieved in the previous time step, the defective temperature profile will be used in the next time step, thus degrading calculation operations thereafter as errors are inherent and accumulating. These issues reduce the method's efficiency and accuracy. To compare the proposed scheme with the existing iterative method, MATLAB built-in optimization functions [11] were used. The initial surface heat flux values were guessed and used to calculate the internal temperature distribution using the finite difference method. Once the temperature distribution was obtained, it could be compared to the temperature values from the thermocouples. The difference, as known as the error, could thus be derived. MATLAB built-in optimization functions were used to search for the optimal surface temperatures (the fourth boundary condition) to minimize the error value. When the minimum error value and appropriate heat flux values are determined, the RMSE values were calculated for thermocouples 4 to 8. The traditional IHCP method was tested using two different settings. First, the heat flux was set with a lower bound of -0.3 MW/m^2 and an initial guess of 3 MW/m^2. Second, the heat flux value was set with a lower bound and an initial guess of 17 MW/m^2. Traditional IHCP methods used approximately 5 hours to complete

the calculation process, as opposed to about 1 minute for the novel IHCP calculation scheme. Also, as shown in Fig. 7, the RMSE values obtained from the traditional IHCP method are much higher than those from the novel IHCP method. Thus, we can conclude that the proposed calculation scheme can provide efficient and accurate results.

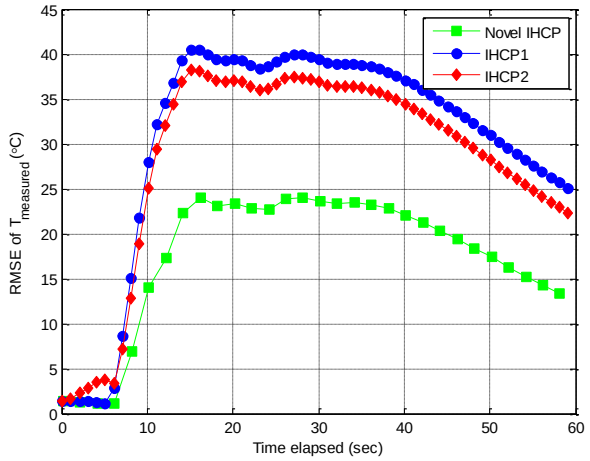

Figure 7. RMSE of novel IHCP and traditional IHCP. The green line presents RMSE values from the proposed novel IHCP method, while the blue and red lines respectively present RMSE values of traditional IHCP method with initial heat flux guess 3 MW/m2 and 17 MW/m2.

Best combinations

Experiments for various impinging patterns and positions were performed, with results shown as RMSE histories. Lower RMSEs represent a more accurate calculation. Figures 8 to 10 show the RMSE results from various impinging positions (P1, P2, and P3, respectively). For each figure, three figures from top to bottom are from results of various impinging patterns: inline jet (flat spray), jet (solid-stream jet), and spray (full-cone spray).

Algorithm 1 is good for impinging positions 1 and 3, while Algorithm 2 works best for impinging position 2. All algorithms show no difference for spray system, because of the uniform impinging pattern of the spray. For all three impinging patterns, RMSEs decrease from the impinging positions 1 to 3. The proposed calculation scheme seems to work best when the impinging position is lower. The down-flowing liquid below the impinging position causes an asymmetric heat-flux pattern, and may affect the calculation accuracy. Also, the jet impinging pattern exhibits lower RMSE values than the others. Jet impinging cooling was the most suitable application for the proposed scheme. Algorithm 2 can be considered more suitable for inline jet and jet at position 2. On the contrary, at positions 1 and 3, Algorithm 1 shows the best RMSE for inline jet and jet. The best combination of the impinging pattern, impinging position, and the unknown boundary condition derivation algorithm is listed in Table 1. Figure 11 shows RMSE curves applied with best algorithm.

After deriving the internal temperature distribution, the calculated data can be used to estimate the heat flux on the fourth boundary. The heat flux histories at the impinging point are shown in Fig. 12. Surface heat flux profiles at specific times can be seen in Fig. 13. While the surface heat flux profile is not very easily observed or measured, the plotted profiles seem to be valid and physically meaningful.

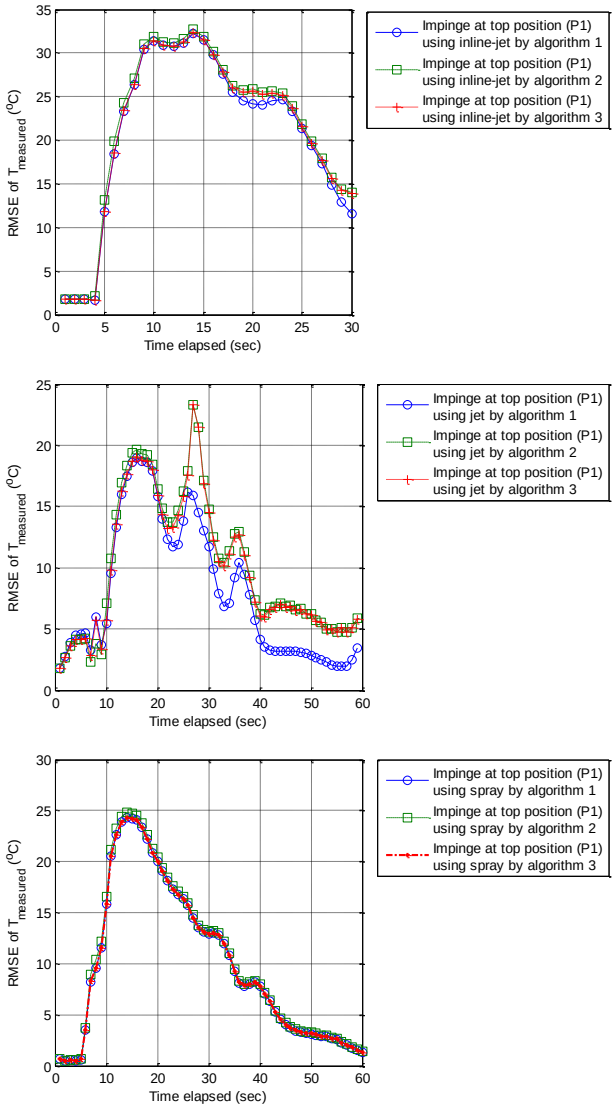

Figure 8. Impinging at top position (P1) by three impinging patterns: inline jet, jet, and spray (top to bottom).

Known suitable applications and shortcomings of the proposed scheme

Comparing the RMSE values from results of jet and of spray impinging shows that simpler impinging patterns produce fewer errors. The jet impinging area can be treated as a point contact, while spray impinging area is a circle. Because of the simple impinging patterns of jets, the surface temperature profiles predicted by the proposed algorithms are close to the actual ones, and lead to better performance from the proposed calculation

scheme. For this reason, it can be concluded that the three unknown boundary condition derivation algorithms tend to precisely simulate temperature profiles for the systems with a simple impinging area.

Due to gravity, the liquid might attach to the surface of the portion below the impinging point. Sometimes the upper part of the impinging surface was not wet, but the lower part was covered by a film of water. This might result in an asymmetric surface heat flux, which differs from the three unknown boundary condition derivation algorithms, leading to imprecise predictions. Therefore, the derived profile would not fit the real surface temperature distribution. Consequently, when the impinging position is low and most of the impinging surface is wet, the scheme produces less RMSEs.

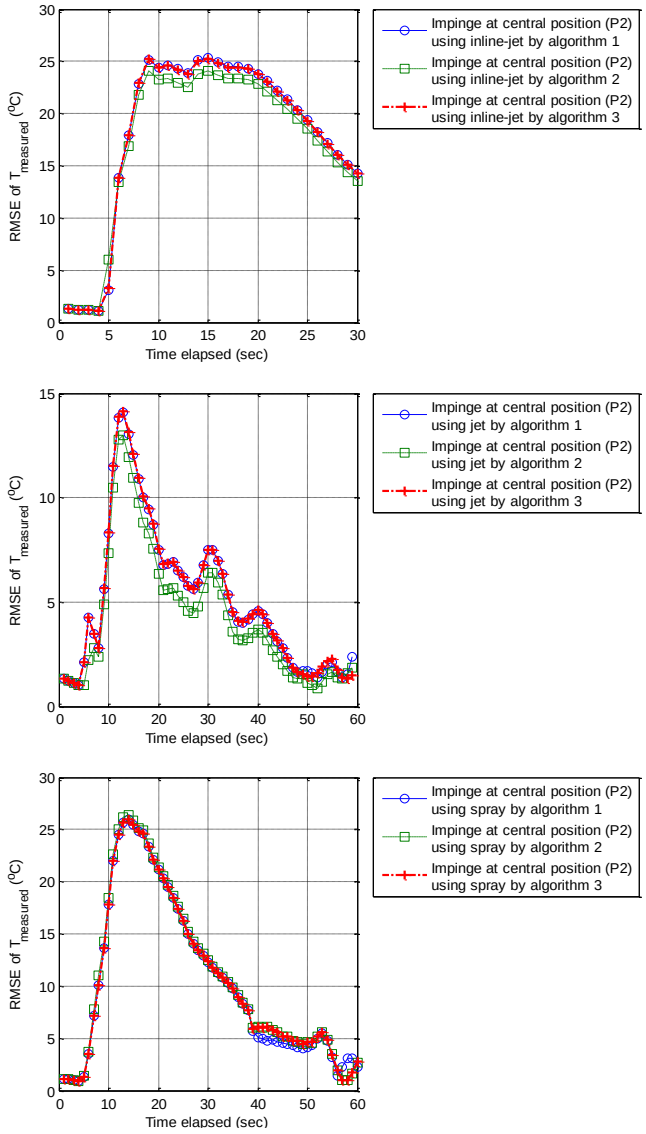

Figure 9. Impinging at central position (P2) by three impinging systems. Figures from top to bottom are for inline jet, jet, and spray impinging patterns.

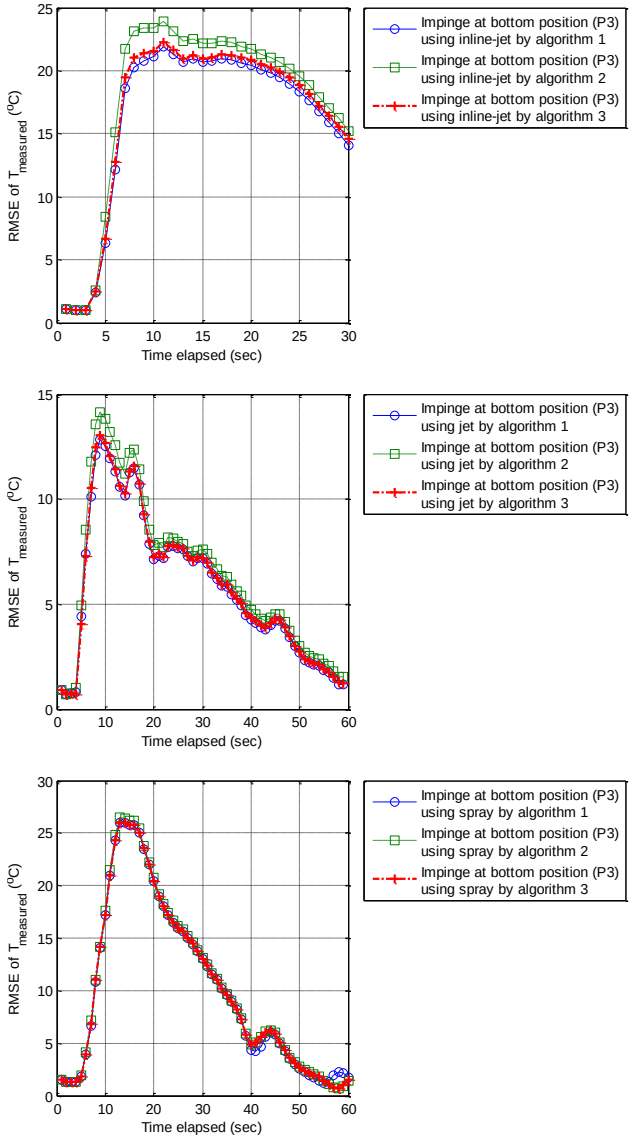

Figure 10. Impinging at bottom position (P3) by three impinging patterns. Figures from top to bottom are for inline jet, jet, and spray impinging patterns.

The most important source of errors is the derived surface temperature profile. Figure 14 demonstrates an abnormal temperature profile for two consecutive time steps. For Algorithms 1 and 2, the situation is more frequent. When the temperature readings from the locations near the impinging surface drop quickly, some negative heat flux can usually be derived near the two edges of the heat flux profile. Abnormal negative values are derived from the numerical calculation, but physically impossible.

The finite difference method used in the proposed scheme always leads to some degree of error. Several continuous properties are converted into discrete ones or Taylor series, thus errors exist in every calculation process. The errors are transmitted and accumulated, thus interior nodes are less accurate than the nodes near the surface.

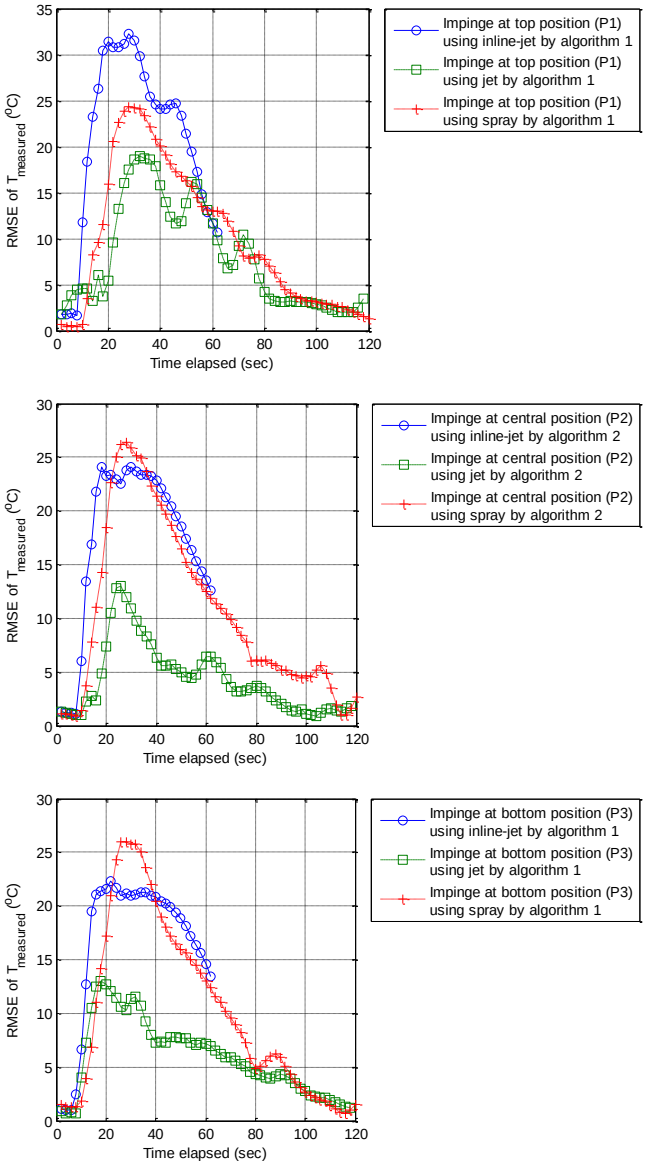

Figure 11. Comparisons between combinations of various impinging patterns and algorithms under best conditions.

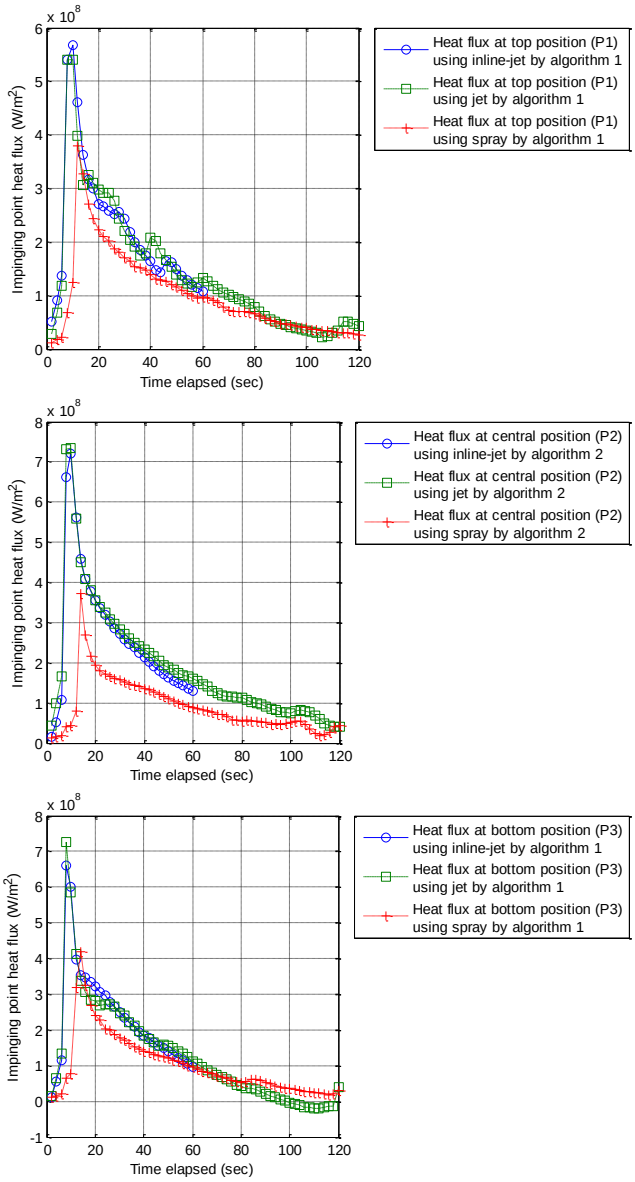

Figure 12. Surface heat flux histories at impinging points for the three impinging patterns with the best surface temperature derivation algorithm. Figures from top to bottom are for impinging points from top to bottom.

Table 1. Combination of operating parameters in this study. * denotes the most suitable algorithm for that combination.

	Inline Jet (Flat Spray)		Jet (Solid-Steam Jet)		Spray (Full-Cone Spray)	
Position1	Algorithm 1	*	Algorithm 1	*	Algorithm 1	*
	Algorithm 2		Algorithm 2		Algorithm 2	*
	Algorithm 3		Algorithm 3		Algorithm 3	*
Position2	Algorithm 1		Algorithm 1		Algorithm 1	*
	Algorithm 2	*	Algorithm 2	*	Algorithm 2	*
	Algorithm 3		Algorithm 3		Algorithm 3	*
Position3	Algorithm 1	*	Algorithm 1	*	Algorithm 1	*
	Algorithm 2		Algorithm 2		Algorithm 2	*
	Algorithm 3		Algorithm 3		Algorithm 3	*

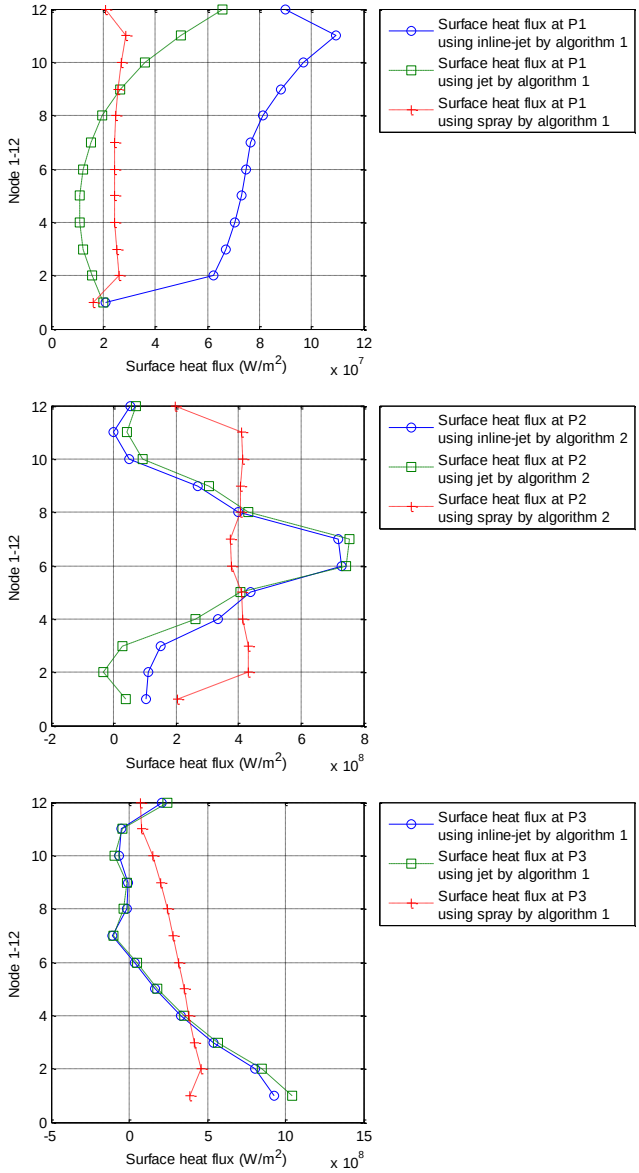

Figure 13. Surface heat flux profile of three impinging patterns using the best algorithms. Figures from top to bottom are for different timing (5, 15, and 25 seconds following process start) during the impinging process.

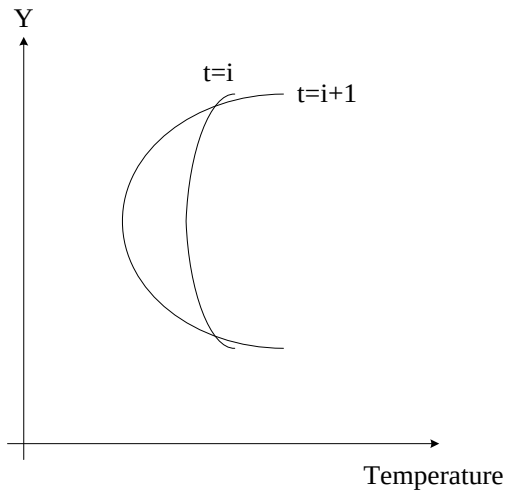

Figure 14. Schematic for inappropriate surface temperature curve.

Conclusions

This study proposes a novel IHCP calculation scheme. Based on the measured data, three algorithms were proposed to derive the unknown boundary condition. Once the last boundary condition was obtained, the conduction problem is no longer inversed, and can be solved without tedious multiple iterations.

An impinging cooling apparatus was constructed to demonstrate the usage of the calculation scheme. Three impinging patterns were tested, including inline jet, jet, and spray. Three impinging positions were also explored. The most suitable unknown boundary condition derivation algorithm for each impinging pattern or for each impinging positions was suggested.

Based on the comparison between solved and measured temperatures, the proposed scheme was shown to be reliable and produced results with a smaller degree of error. A much shorter processing time was required than that using traditional IHCP solving methods. The proposed calculation scheme was also shown to effectively derive surface heat flux for impinging cooling problems.

References

[1] C. H. Liebert, "Measurement of local high-level, transient surface heat flux," National Aeronautics and Space Administration, Cleveland, OH, NASA Techanical Paper 2840, 1988.

[2] A. Alkidas and J. Myers, "Transient heat-flux measurements in the combustion chamber of a spark-ignition engine," *Journal of Heat Transfer,* vol. 104, no. 1, pp. 62-67, 1982. doi: 10.1115/1.3245069

[3] V. K. Zantsev, "Application of inverse heat-conduction problems in experimental investigations of the heat exchange of casting units of furnaces," *Journal of Engineering Physics and Thermophysics,* vol. 45, no. 5, pp. 13-18, 1983. doi: 10.1007/BF01254744

[4] G. Stolz Jr, "Numerical solutions to an inverse problem of heat conduction for simple shapes," *Journal of Heat Transfer,* vol. 82, no. 1, pp. 20-25, 1960. doi: 10.1115/1.3679871

[5] B. R. Bass and L. J. Ott, "Finite element formulation of the two-dimensional nonlinear inverse heat conduction problem," in proceeding of *ASME Century 2 EmergingTtechnology Conference*, San Francisco, CA, USA, 10-22 Aug, 1980, CONF-800804-33.

[6] Y. Liu and D. A. Murio, "Numerical experiments in 2-

D IHCP on bounded domains Part I: The "interior" cube problem," *Computers & Mathematics with Applications,* vol. 31, no. 1, pp. 15-32, 1996.

[7] W.-K. Yeung and T.-T. Lam, "Second-order finite difference approximation for inverse determination of thermal conductivity," *International Journal of Heat and Mass Transfer,* vol. 39, no.17, pp. 3685-3693, 1996.
doi: 10.1016/0017-9310(96)00028-2

[8] N. V. Shumakov, "A method for experimental study of the process of heating a solid body," *Soviet Physics-Technical Physics,* pp. 771-781, 1957.

[9] J. V. Beck, "Surface heat flux determination using an integral method," *Nuclear Engineering and Design,* vol. 7, no. 2, pp. 170-178, 1968.
doi: 10.1016/0029-5493(68)90058-7

[10] J. V. Beck, "Nonlinear estimation applied to the nonlinear inverse heat conduction problem," *International Journal of Heat and Mass Transfer,* vol. 13, no. 4, pp. 703-716, 1970.
doi: 10.1016/0017-9310(70)90044-X

[11] X.-Y. WU, "Investigation of the inverse heat conduction problems using the hybrid inverse method with experimental data," Ph.D. dissertation, Department of Mechanical Engineering, National Cheng Kung University, Tainan, Taiwan, 2006.

[12] Y.-K. Wang, "A novel numerical method to derive the surface heat flux of liquid impingement cooling," M.S. thesis, Department of Industrial Mechanical Engineering, National Taipei University of Technology, Taipei, Taiwan, 2009.